scientific reports

OPEN

Understanding the antiviral effects of RNAi-based therapy in HBeAg-positive chronic hepatitis B infection

Sarah Kadelka[1], Harel Dahari[2] & Stanca M. Ciupe[1]✉

The RNA interference (RNAi) drug ARC-520 was shown to be effective in reducing serum hepatitis B virus (HBV) DNA, hepatitis B e antigen (HBeAg) and hepatitis B surface antigen (HBsAg) in HBeAg-positive patients treated with a single dose of ARC-520 and daily nucleosidic analogue (entecavir). To provide insights into HBV dynamics under ARC-520 treatment and its efficacy in blocking HBV DNA, HBsAg, and HBeAg production we developed a multi-compartmental pharmacokinetic–pharamacodynamic model and calibrated it with frequent measured HBV kinetic data. We showed that the time-dependent single dose ARC-520 efficacies in blocking HBsAg and HBeAg are more than 96% effective around day 1, and slowly wane to 50% in 1–4 months. The combined single dose ARC-520 and entecavir effect on HBV DNA was constant over time, with efficacy of more than 99.8%. The observed continuous HBV DNA decline is entecavir mediated, the strong but transient HBsAg and HBeAg decays are ARC-520 mediated. The modeling framework may help assess ongoing RNAi drug development for hepatitis B virus infection.

Treatment options for chronic hepatitis B virus (HBV) infections are limited to two main drug groups: pegylated interferon-α (IFN) and nucleos(t)ide analogues (NAs)[1–3]. Treatment with IFN induces antiviral activity, immunomodulatory effects, and robust off-treatment responses. These responses, however, vary among patients and induce *functional cure*, defined as hepatitis B surface antigen (HBsAg) loss, in only $10 - 20\%$ Caucasian patients and less than 5% Asian patients. Moreover, IFN treatment is poorly tolerated[4–6]. By contrast, treatment with NAs is well tolerated and can be life-long but has limited effect in reducing serum HBsAg and hepatitis B e-antigen (HBeAg) production and, in limiting hepatitis B covalently closed circular DNA (cccDNA) persistence and HBV DNA integration[1,7,8], all of which play important roles in chronic infections. HBeAg is thought to induce T cell tolerance to both e- and core antigens and to be an important reason for viral persistence[9]. HBsAgs, besides being used for virion envelopes, form empty non-infectious subviral particles (*i.e.* without viral genome) whose numbers are at least 1,000-folds higher than those of virions[10], and may serve as decoy for antibody responses[11]. Moreover, they are also assumed to be involved in T cell exhaustion[12,13]. Functional cure has been proposed as a desirable outcome of treatment. None of the currently licensed therapies can produce this result for a large fraction of chronically infected patients. There is therefore a need for new therapies that target HBsAg production and/or its clearance from circulation[14,15].

RNA interference (RNAi) technology has the ability of silencing specific genes and can, therefore, be used for treatment against a large array of infectious agents (see[16] for a review on RNAi-based therapies). For hepatitis B infection, small interfering RNAs were designed to hybridize with HBV mRNA inside an infected hepatocyte and, as a result, induce its degradation[17–19]. ARC-520, the first such small interfering RNA to be tested in clinical trials, was designed with the aim of knocking down the expression of all HBV mRNA, including HBsAg proteins. Experiments in mice and chimpanzees, and a phase II clinical study in patients (Heparc-2001) showed potential for ARC-520 induced HBeAg, HBsAg and HBV DNA titers reduction[17,20,21]. The Heparc-2001 study showed differential HBsAg reduction among patients based on their HBeAg status and prior exposure to traditional therapy such as NAs[20]. While ARC-520 has been terminated due to delivery-associated toxicity[20], overall results indicate that RNAi-based therapy has the potential of reducing HBsAg and inducing functional cure[16,21,22] regardless of the patient's HBeAg status[23,24].

[1]Department of Mathematics, Virginia Tech, Blacksburg, VA 24060, USA. [2]Program for Experimental and Theoretical Modeling, Stritch School of Medicine, Loyola University Chicago, Maywood, IL 60153, USA. ✉email: stanca@vt.edu

To better understand the effect of RNAi therapies, additional information regarding the host-virus-drug dynamics and therapy outcomes are needed. In this study, we developed mathematical models that best reproduce observed HBV DNA, HBsAg and HBeAg kinetics following a single dose of ARC-520 in five HBeAg-positive patients from the Heparc-2001 study. Mathematical models of hepatitis B infection have been used to study the dynamics of acute, chronic, and occult HBV infections[25–29], anti-HBV therapy[14,30–35], cell-to-cell transmission[36], intracellular interactions[36–38], cellular immune responses[26,30,39–41], antibody-mediated immune responses[11,38,42], HBeAg[38,43,44], and HBeAb[38] dynamics. We build on previous modeling work, consider the interaction between HBV DNA, HBsAg and HBeAg titers in the presence of a single dose RNAi-based therapy, and use the model to run *in silico* experiments to predict individual contributions of different drug effects on the dynamics for HBsAg titers.

Methods

Patient data.
We use published data from five HBeAg-positive, treatment-naive chronic hepatitis B patients (cohort 7 in[20]), which are the ones that best responded to ARC-520 therapy. Data consists of serum HBV DNA titers (in IU/ml), HBsAg, and HBeAg concentration (in IU/ml) measured at $t_i = \{-8, 0, 2, 7, 14, 21, 28, 42, 56, 84\}$ days, where $i = \{-1, \ldots, 8\}$ and $t_0 = 0$ is the day when both daily NA entecavir (ETV) and a single intravenous ARC-520 injection (inoculum of 4 mg/kg) are administered.

Pharmacokinetics–pharamcodynamics model.
We are interested in determining the mechanisms underlying the observed HBV DNA, HBsAg and HBeAg kinetics under combined ETV and ARC-520 therapy. We develop a mathematical model that considers the interactions between infected hepatocytes, I (in cells per ml); total intracellular HBV DNA, D (in copies per ml); serum HBV DNA, V (in IU per ml); serum HBsAg, S (in IU per ml); and serum HBeAg, E (in IU per ml). We assume that infected cells decay at per capita rate δ, and we exclude cell proliferation (we will relax this assumption later on). We assume intracellular HBV DNA is synthesized at rate α and is lost at constant per capita rate c_D. The replication rate α summarizes various steps that are not modeled explicitly, such as the transcription of pregenomic RNA (pgRNA) from cccDNA, and the generation of single stranded DNA by reverse transcription. Intracellular HBV DNA is assembled and released into blood as free virions at rate p which are cleared at rate c. To account for the different units of intracellular and serum virus, we use the conversion factor $\xi = 1/5.3$ IU/copies[45]. Lastly, we assume HBsAg and HBeAg are transcribed from cccDNA inside infected hepatocytes and then released into blood at rates p_S and p_E, respectively, and are cleared at per capita rates d_S and d_E, respectively. The model is given by the following model:

$$\frac{dI}{dt} = -\delta I,$$
$$\frac{dD}{dt} = \alpha - (p + c_D)D,$$
$$\frac{dV}{dt} = \xi p DI - cV, \tag{1}$$
$$\frac{dS}{dt} = p_S I - d_S S,$$
$$\frac{dE}{dt} = p_E I - d_E E.$$

Patients were administered daily nucleoside analogous treatment with entecavir starting at day $t_0 = 0$. ETV is known to block reverse transcription of HBV DNA, and therefore inhibit HBV DNA synthesis. We model this (see model (5)) as a constant reduction of the HBV DNA synthesis rate α to $(1 - \epsilon)\alpha$, where $0 \leq \epsilon \leq 1$ is the ETV efficacy. Experimental studies in humanized mice have shown that serum HBV DNA declines in biphasic manner while HBV-infected cell are not lost in the first months following NA treatment initiation[46,47]. To account for the biphasic HBV DNA decay in the absence of infected cell killing, we assume that ETV has additional time-dependent inhibitory effects on intracellular HBV DNA synthesis and model it by decreasing α further to $\alpha_{treat}^{ETV} = \alpha e^{-gt}(1 - \epsilon)$, where $g \geq 0$ is a constant and t is the time in days post ETV initiation. Moreover, a single ARC-520 dose was administered at time $t_0 = 0$. Unlike ETV, which was given daily, we model the build-up and clearance of ARC-520 pharmacokinetics over time by considering a two-compartment pharmacokinetic model consisting of drug quantity in the plasma and liver, C_p and C_e, respectively[48]. The inoculum $C_p(0) = C_0$ decays exponentially at rate $d = \tilde{d} + k_{eo}$, where $\tilde{d}$ is the plasma drug degradation rate and k_{eo} is the absorption into the liver rate. The drug in the liver decays at rate k_{eo}, identical with the absorption rate[49]. Following these assumptions, the pharmacokinetic model has the form:

$$\frac{dC_p}{dt} = -\tilde{d}C_p - k_{eo}C_p,$$
$$\frac{dC_e}{dt} = k_{eo}C_p - k_{eo}C_e, \tag{2}$$

with initial conditions $C_p(0) = C_0$ and $C_e(0) = 0$. This is a linear model which can be solved to give solutions:

$$C_p(t) = C_0 e^{-dt},$$
$$C_e(t) = \frac{C_0 k_{eo}}{d - k_{eo}}(e^{-k_{eo}t} - e^{-dt}). \tag{3}$$

Lastly, we assume the relationship between the drug quantity in the liver $C_e(t)$ and drug efficacy $\eta_i(t)$ to be given by:

$$\eta_i(t) = \frac{\eta_{max} \times C_e(t)}{EC_{50,i} + C_e(t)}, \tag{4}$$

where $\eta_{max} = 1$ is the maximum drug efficacy, $EC_{50,i}$ are drug quantities that yield half-maximal effects, and $i = \{1, 2, 3\}$ are the infectious events that are affected by ARC-520 therapy, *i.e.*, the transcription of HBV DNA, the transcription of HBsAg, and the transcription of HBeAg, respectively. The effects of ARC-520 on intracellular HBV DNA, HBsAg and HBeAg are modeled as the reduction of intracellular HBV DNA synthesis α to $\alpha_{treat}^{ARC} = (1 - \eta_1)\alpha$, HBsAg production from p_S to $p_{S,treat} = (1 - \eta_2)p_S$, and of HBeAg production from p_E to $p_{E,treat} = (1 - \eta_3)p_E$, respectively. Considered together, models (1) and (4) give the following pharmacokinetics–pharamcodynamics (PK/PD) model:

$$\frac{dI}{dt} = -\delta I,$$
$$\frac{dD}{dt} = (1 - \epsilon)(1 - \eta_1(t))e^{-gt}\alpha - (p + c_D)D,$$
$$\frac{dV}{dt} = \xi p D I - cV, \tag{5}$$
$$\frac{dS}{dt} = (1 - \eta_2(t))p_S I - d_S S,$$
$$\frac{dE}{dt} = (1 - \eta_3(t))p_E I - d_E E.$$

Data fitting. We used published kinetic HBV DNA, HBsAg, HBeAg data in serum measured from five HBeAg-positive, treatment-naive chronic hepatitis B patients as described in the 'Patient data' section.

Parameter values. We assume that, prior to therapy initiation, model (5) describes a persistent chronic infection and is at the quasi-equilibrium, given by the initial values $I(0) = I_0$, $D(0) = D_0$, $V(0) = V_0$, $S(0) = S_0$ and $E(0) = E_0$. Initial values for HBV DNA, $V(0) = V_0$; HBsAg, $S(0) = S_0$; and HBeAg, $E(0) = E_0$, are set to the patient data prior to the start of therapy, $t_{-1} = -8$, (day eight prior to the ARC-520 injection). The percentage of HBV-infected hepatocytes is reported to vary between $18 \pm 12\%$ in chronic HBsAg carriers[50,51] and 99% in acute infections[26,52]. Without loss of generality, we arbitrary assume that 50% of hepatocytes are infected at the beginning of treatment. Liver contains approximately 2×10^{11} hepatocytes, which, when distributed throughout 15 liters of extracellular fluid, gives a total hepatocyte concentration $T_{max} = 1.4 \times 10^7$ cells/ml[53]. We set the initial infected hepatocyte population to $I_0 = 0.5T_{max}$. Lastly, the pre-treatment level of intracellular HBV DNA in HBeAg positive patients is set to $D_0 = 225/(I_0/T_{max}) = 450$ copies/ infected cell, as in[54].

Since we assume that model (5) is in chronic equilibrium (for the additional assumption $\delta = 0$) before the therapy initiation, parameters α, p, p_S, p_E are fixed according to the following formulas:

$$\alpha = (p + c_D)D_0, \quad p = cV_0/(\xi D_0 I_0), \quad p_S = d_S S_0/I_0, \quad p_E = d_E E_0/I_0. \tag{6}$$

We start by ignoring the dynamics of infected cells, such as infection of susceptible cells and/or infected cell proliferation (we will relax this assumption in later sections), and assume that infected cells decay due to natural death and immune mediated killing at per capita rate $\delta = 4 \times 10^{-3}$ per day, corresponding to a life-span of 250 days (we will later investigate the effect of increasing the killing rate, to include increased immune mediated killing or RNAi induced toxicity and death). The estimated half-life of intracellular HBV DNA is 24 h[55], which corresponds to the intracellular HBV DNA decay rate $c_D = 0.69$ per day. ARC-520's half-life has been reported to range between 3 and 5 h[56], corresponding to decay rates $3.3 < d < 5.5$ per day; we fix $d = 4$ per day. Lastly, we set the initial ARC-520 quantity to the trial dose of $C_0 = 4$ mg/kg.

The unknown parameters are **parm** $= \{g, c, d_S, d_E, \epsilon_T, EC_2, EC_3, k_{eo}\}$. Here, $(1 - \epsilon_T) = (1 - \epsilon)(1 - \eta_1(t))$ accounts for the total drug effect on HBV DNA production. Since preliminary simulations (not shown) indicate that $\eta_1(t)$ is time independent, we cannot separate the ETV effects $1 - \epsilon$ from the ARC-520 effects $1 - \eta_1(t)$. We lump them together, and assume a total drug effect, which ranges between $0.9 < \epsilon_T < 1$. The other parameter ranges are found as follows. The time-dependent inhibitory effects of treatment on intracellular HBV DNA production, g, was estimated from HBV infected humanized mice treated with NA to range between 0.059 and 0.42 per day. We expand this range by searching over the parameter space $0 < g < 1$. There is a wide range of estimates for the free virus clearance rate in serum: as low as 0.69 per day[25,33,57]; and as high as 21.7 per day[58]; we search the entire $0 < c < 100$ parameter space. The decay rate of HBsAg is bounded between $0 < d_S < 200$ per day, containing previous estimates ranging between 0.057 to 0.58 per day[59,60]. In previous modeling work[44,61] HBeAg decay rate d_E was set to 0.3 per day. We allow for a larger range $0 < d_E < 200$ per day, corresponding to half-lives greater than 5 minutes. We assume that the drug absorption rate k_{eo} ranges between $0 < k_{eo} < 1$ per

Variables	Description	Units		Initial values
I	Infected hepatocytes	cells/ml		0.7×10^6
D	Intracellular HBV DNA	copies/cell		450[54]
V	Free virions	IU/ml		Data at time $t_{-1} = -8$
S	Serum HBsAg	IU/ml		Data at time $t_{-1} = -8$
E	Serum HBeAg	IU/ml		Data at time $t_{-1} = -8$
Parameters	Descriptions	Units	Default values / range	Reference
δ	Infected cells decay rate	1/day	4×10^{-3}	
g^*	Inhibitory effects on intracellular HBV production during treatment	1/day	$[0, 1]$	
α	Intracellular HBV DNA synthesis rate	Copies/(cell×day)	$(p + c_D)D_0$	
c_D	Intracellular HBV DNA decay rate	1/day	0.69	[55]
ξ	Conversion factor	IU/copies	$1/5.3$	[45]
p	Intracellular HBV DNA release rate	1/day	$cV_0/(\xi D_0 I_0)$	
c^*	Free virion clearance rate	1/day	$[0, 100]$	
p_S	HBsAg production rate	IU/(cell×day)	$d_S S_0/I_0$	
p_E	HBeAg production rate	IU/(cell×day)	$d_E E_0/I_0$	
d_S^*	HBsAg decay rate	1/day	$[0, 200]$	
d_E^*	HBeAg decay rate	1/day	$[0, 200]$	
ϵ_T^*	Combined ETV and ARC-520 efficacy	unitless	$[0.9,1]$	
C_0	Initial plasma drug quantity	mg/kg	4	[20]
d	ARC-520 decay rate	1/day	4	[56]
EC_2^*	ARC-520 Quantity where η_2 is half maximal	mg/kg	$[10^{-7}, 1]$	
EC_3^*	ARC-520 Quantity where η_3 is half maximal	mg/kg	$[10^{-7}, 1]$	
k_{eo}^*	Drug absorption rate	1/day	$[0,1]$	

Table 1. Variables and parameters in model (5). Parameters indicated by a ⋆ are fitted within the given range.

day. Since ARC-520 was reported to have long lasting effects[56], we assume a large range for the half-maximal quantity EC_i; between $10^{-7} < EC_i < 1$ mg/kg. These ranges are summarized in Table 1.

Optimization algorithm. We estimate the unknown parameters **parm** given in Table 1 by minimizing the least squares functional:

$$SSQ = \sum_{P \in \{V,S,E\}} \left(\sum_{i=1}^{N=8} \left(\log_{10} P(t_i) - \log_{10} P_{data}(t_i) \right)^2 \right)^{1/2}, \tag{7}$$

for each patient. Functional SSQ describes the distance between HBV DNA, HBsAg, and HBeAg titers $V_{data}(t_i)$, $S_{data}(t_i)$, $E_{data}(t_i)$ at times t_i ($i = \{1, \ldots, 8\}$) and populations $V(t_i)$, $S(t_i)$ and $E(t_i)$ as given by model (5) at times t_i ($i = \{1, \ldots, 8\}$). As described previously (see Eq. (6)), the before treatment titers at $t_{-1} = -8$ days are used to determine parameters α, p, p_S, p_E such that the model's equilibrium matches the titers exactly. Since we assume that the model stays in equilibrium until treatment initiation, we ignore the titers at time $t_0 = 0$ days. Lastly, it should be noted that we assign the same weight to errors in HBV DNA, HBsAg, and HBeAg. Within the parameter space defined in Table 1, we determine optimal parameter fits for each patient by following four steps (code available upon publication):

1. We create 100 parameter sets using the Latin hypercube samples (LHS) *Matlab* routine *lhsdesign*, with random number generator seed two and uniform probability density distribution on each parameter interval. Since the parameter space spans several orders of magnitude in EC_2 and EC_3 directions, we replace them with $EC_2 = 10^{\widetilde{EC_2}}$ and $EC_3 = 10^{\widetilde{EC_3}}$. Thus, instead of sampling EC_2 and EC_3 in $[10^{-7}, 1]$, we sample $\widetilde{EC_2}$ and $\widetilde{EC_3}$ in $[-7, 0]$. Our preliminary work showed that $\epsilon_T \approx 1$ often yields the best results. Therefore, we replace $(1 - \epsilon_T) = 10^{\widetilde{\epsilon_T}}$ and sample $\widetilde{\epsilon_T}$ in the parameter space $[-8, -1]$.

2. HBV DNA dynamics do not influence HBsAg and HBeAg dynamics. Therefore, we minimize
$SSQ_V = \left(\sum_{i=1}^{N=8} \left(\log_{10} V(t_i) - \log_{10} V_{data}(t_i) \right)^2 \right)^{1/2}$ and $SSQ_{S,E} = \sum_{P \in \{S,E\}} \left(\sum_{i=1}^{N=8} \left(\log_{10} P(t_i) - \log_{10} \right.$
$\left. P_{data}(t_i) \right)^2 \right)^{1/2}$ separately over their corresponding parameter sets **parm**$_V = \{g, c, \epsilon_T\}$ and **parm**$_{SE} = \{d_S, d_E, EC_2, EC_3, k_{eo}\}$, respectively. We split the LHS into LHS$_V$ and LHS$_{S,E}$ containing the respec-
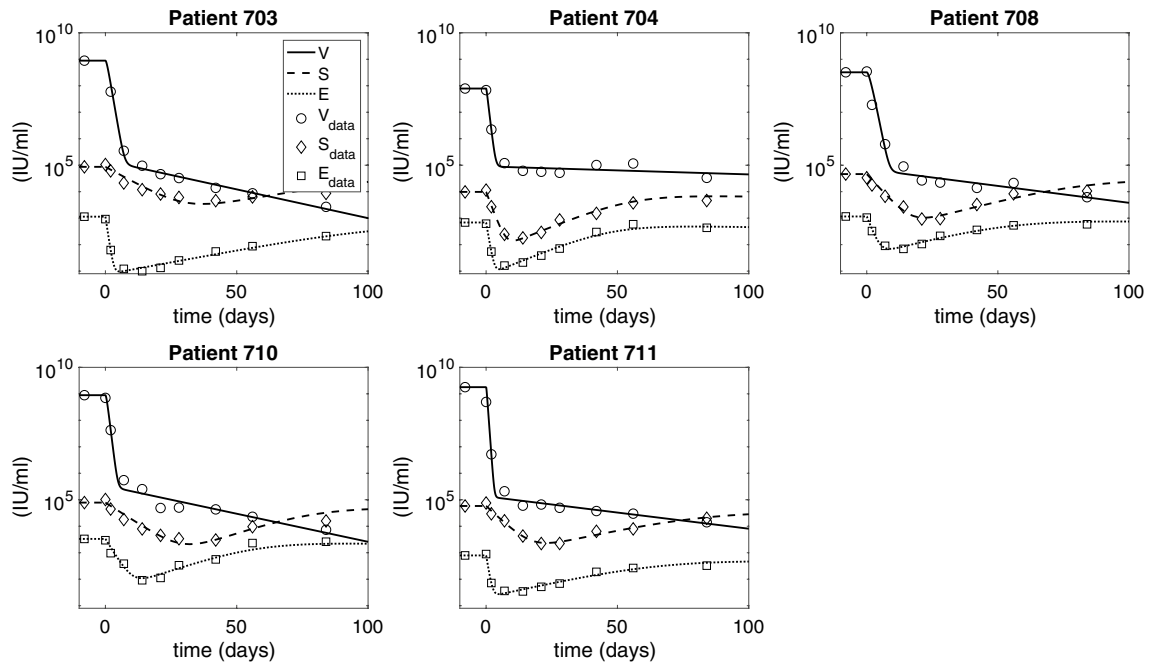
nature research 4

Figure 1. HBV DNA, HBsAg, and HBeAg dynamics over time as given by model (5) (solid curves) versus data (circles). The parameters are given in Tables 1 and 2.

tive initial parameter guesses and, using *Matlab's fmincon* routine to minimize SSQ_V and $SSQ_{S,E}$ within the parameter space in Table 1, obtain 100 *optimal* **parm**$_V$ and **parm**$_{S,E}$ parameter sets.

3. Of the 2×100 *optimal* parameter sets found in part two, we choose the ones yielding minimal $SSQ = SSQ_V + SSQ_{S,E}$, as the overall optimal parameter set for the given patient.

4. To obtain confidence intervals for the optimal parameter estimates p_{opt} for each patient, we employ a boot-strapping technique. We assume that the best fit parameters yield the true dynamics, and that any discrepancy from the data is due to measurement errors. First, we calculate the residuals

$$
\begin{aligned}
r_i^V &= \log_{10}(V_{data}(t_i)) - \log_{10}(V(p_{opt}, t_i)), \\
r_i^S &= \log_{10}(S_{data}(t_i)) - \log_{10}(S(p_{opt}, t_i)), \\
r_i^E &= \log_{10}(E_{data}(t_i)) - \log_{10}(E(p_{opt}, t_i)),
\end{aligned}
\tag{8}
$$

between simulated functions and measured data at times t_i ($i = \{1, \ldots, 8\}$). Next, we create 1000 data sets for the HBV DNA, HBsAg, and HBeAg data at times $t_{-1}, \ldots, t_8$, where data at times t_{-1} and t_0 are as before and data at the remaining times are obtained by adding a randomly drawn residual (with repetition) to the true value at each time, *i.e.*

$$
\log_{10}(P_{data}^{new}(t_i)) = \log_{10}(P(p_{opt}, t_i)) + r_{j_{P,i}}^P,
$$

where $P \in \{V, S, E\}$, $i = 1, \ldots, 8$, and $j_{P,i}$ is drawn at random from $\{1, \ldots, 8\}$. Lastly, for each data set, we find a new set of optimal parameters by using *Matlab's fmincon* with initial parameter guess p_{opt} to minimize SSQ_V and SSQ_{SE}, as described in (2.). This yields 1000 sets of parameters (one for each data sets), and the confidence intervals on the optimal parameters p_{opt} are obtained as the ranges from the 2.5th percentiles to the 97.5th percentiles of the 1000 parameter values.

Results

Parameter estimates. The best parameter estimates, the respective errors (SSQ) and the the 95% confidence intervals obtained by bootstrapping, are given in Table 2. Numerical solutions for each population versus data are shown in Fig. 1 (see also Figs. 2, 3, and 4 for zoomed in results). Table 3 gives the parameters obtained from equilibrium conditions (6).

Previously reported virus clearance rates range from 0.69 per day[25,33,57] to 21.7 per day[58]. We estimate average virus clearance rates among the five patients $c = 3.37 \pm 3.38$ per day, corresponding to average life-spans of 7.1 h. The fastest free virus clearance rate, $c = 9.27$ per day (life-span of 2.6 h), occurs in patient 704, who has the lowest pre-treatment virus titer. Assuming 50% of hepatocytes are HBV-infected, we estimate an average intracellular HBV DNA release rate $p = 3.21 \pm 3.54$ per day. Patient 711, who has the highest pre-treatment virus titer, has $p = 9.37$ per day, 2.9 times higher than the average. Under these estimates, the pre-treatment serum virus production rates, pD_0, range between 301.5 and 1260 copies/(infected cell×day) for patients 703–710, similar to the 200–1000 copies/(infected cell×day) reported for acute HBV infection[62]. Patient 711, however, has a pre-treatment
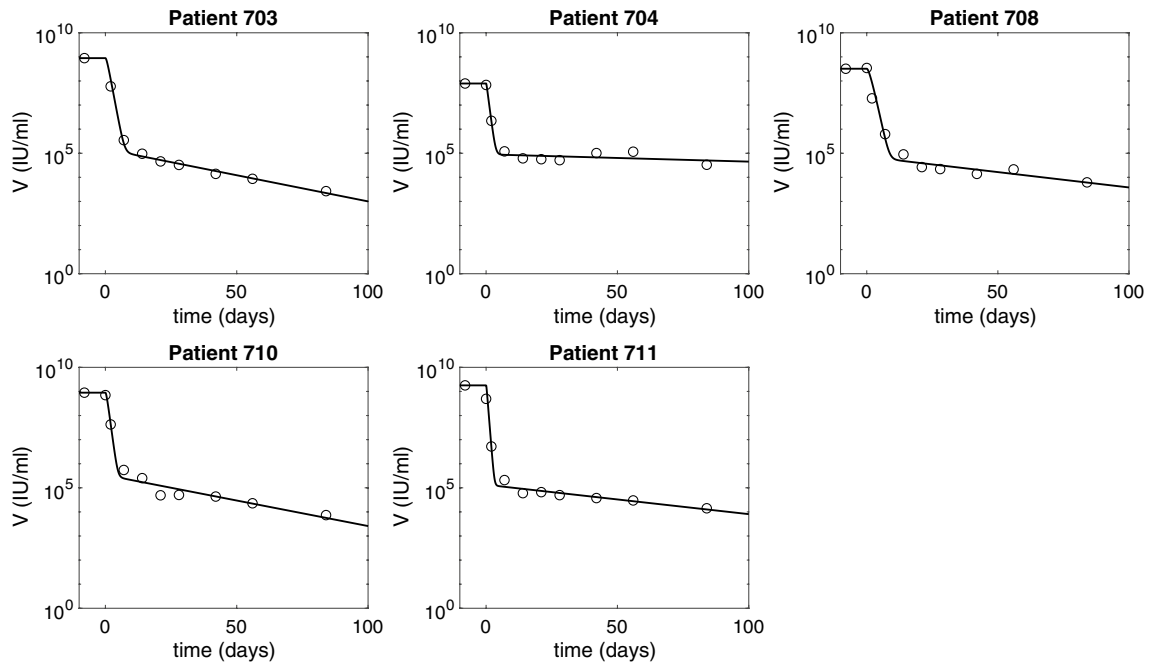
Figure 2. HBV DNA dynamics over time as given by model (5) (solid curves) versus data (diamonds). The parameters are given in Tables 1 and 2.
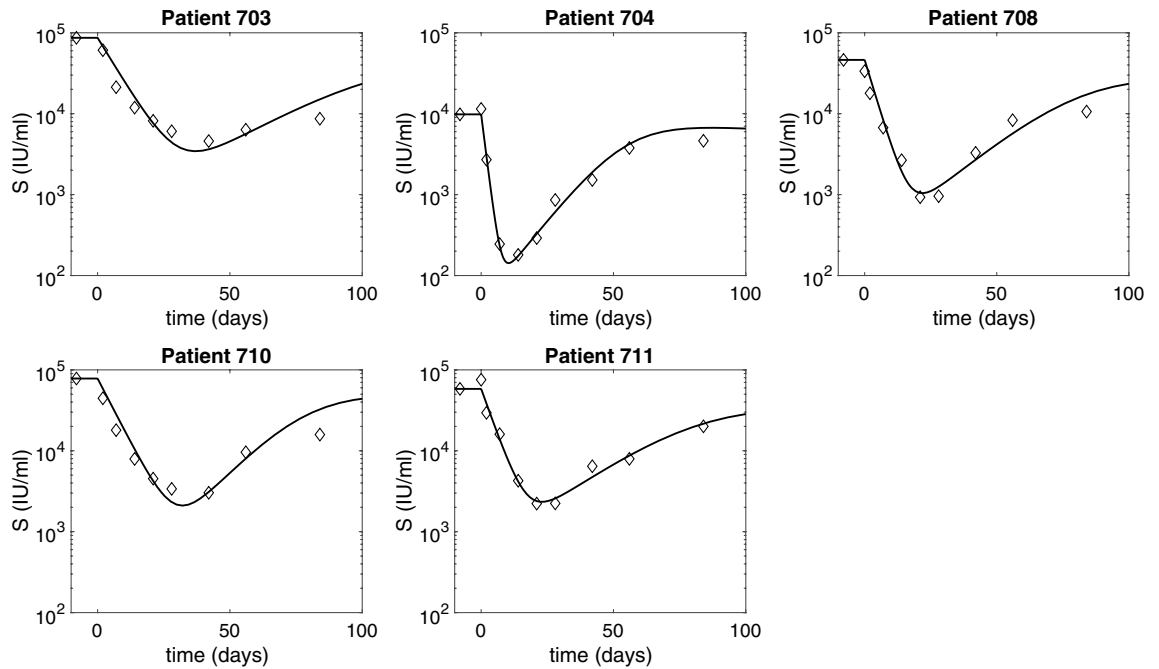

Figure 3. HBsAg dynamics over time as given by model (5) (solid curves) versus data (diamonds). The parameters are given in Tables 1 and 2.

serum virus production rate, $pD_0 = 4216.5$ copies/(infected cell×day), four times larger than in[62]. Intracellular HBV DNA synthesis rates are $\alpha = 1755.66 \pm 1590.21$ copies/(cell× day). As with the serum release rate, patient 711 has 2.6-times higher intracellular HBV DNA synthesis than the average, $\alpha = 4526.23$ copies/(ml× day).

The reported half-life of circulating HBsAg in chronically infected patients is 6.7 days (with a standard deviation of 5.5 days)[59], which corresponds to HBsAg decay rates $0.057 < d_{0,S} < 0.58$ per day. We estimate average HBsAg decay rates $d_S = 0.18 \pm 0.06$ per day, corresponding to HBsAg life-span of 5.6 days for patients 703 and 708-711, and $d_S = 0.6$ per day, corresponding to HBsAg life-span of 1.7 days, for patient 704. The average clearance rates of circulating HBeAg $d_E = 1.05 \pm 0.52$ per day, correspond to HBeAg life-spans ranging between
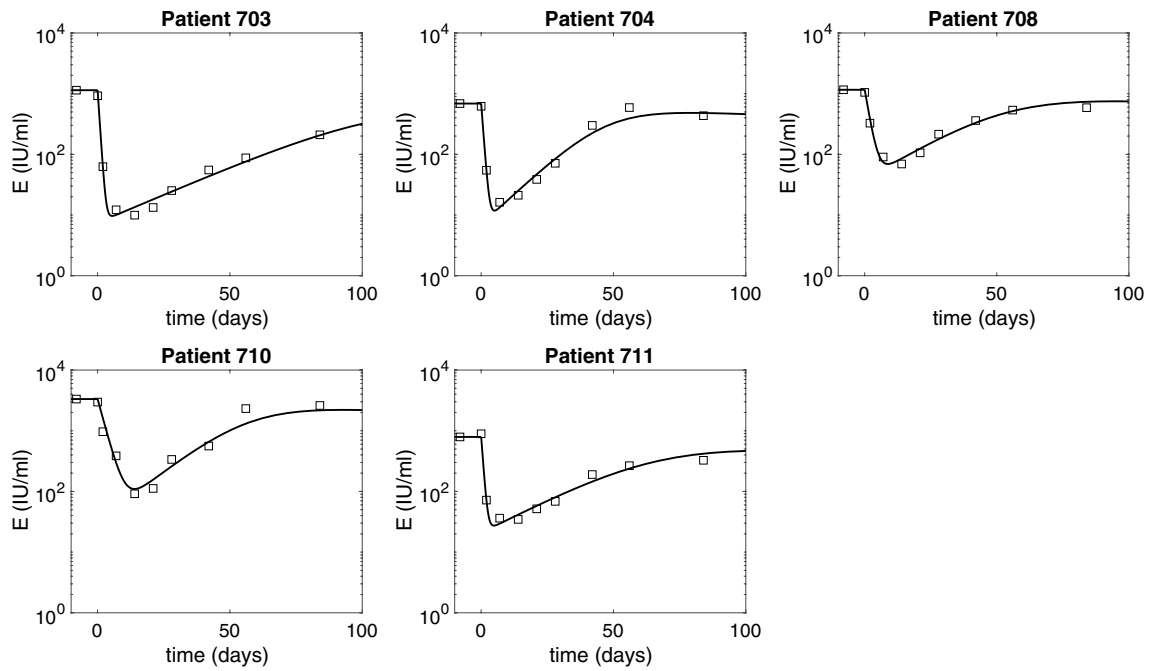
Figure 4. HBeAg dynamics over time as given by model (5) (solid curves) versus data (diamonds). The parameters are given in Tables 1 and 2.

	g	c	d_S	d_E	$1-\epsilon$	EC_2	EC_3	k_{eo}	
	$(\times 10^{-2})$				$(\log_{10})$	$(\log_{10})$	$(\log_{10})$	$(\times 10^{-2})$	
	d^{-1}	d^{-1}	d^{-1}	d^{-1}		mg/kg	mg/kg	d^{-1}	SSQ
703	4.6	1.33	0.12	1.52	−3.8	−3.39	−3.49	4.69	1.03
703	(3.7,5.8)	(1.3,1.6)	(0.11,0.16)	(1.3,1.7)	(−4,−3.6)	(−3.6,−3.2)	(−3.6,−3.4)	(4,5.4)	
704	0.3	9.27	0.6	1.35	−2.94	−3.25	−2.96	9.81	1
704	(0,1.4)	(6.8,11)	(0.5,0.7)	(1.1,1.5)	(−3,−2.7)	(−3.4,−3.2)	(−3,−2.8)	(8.5,11.2)	
708	2.54	1.24	0.25	0.6	−3.67	−3.39	−2.61	6.43	1.42
708	(0.6,5.1)	(1.1,2.5)	(0.2,0.3)	(0.5,0.8)	(−4.2,−3.3)	(−3.6,−3.3)	(−2.7,−2.5)	(5.2,7.7)	
710	4.48	1.87	0.15	0.37	−3.43	−3.73	−3.02	8.3	1.48
710	(2.9,6)	(1.3,2.4)	(0.1,0.18)	(0.2,0.5)	(−3.7,−3.1)	(−4.2,−3.4)	(−3.2,−2.8)	(5.9,11)	
711	2.41	3.12	0.21	1.4	−4.13	−3.14	−2.8	5.55	0.78
711	(1.4,3.2)	(2.8,3.3)	(0.2,0.24)	(1.1,1.7)	(−4.3,−3.9)	(−3.2,−3)	(−2.9,−2.7)	(4.7,6.4)	
MEAN	2.87	3.37	0.27	1.05	−3.59	−3.38	−2.98	6.96	1.14
MEDIAN	2.54	1.87	0.21	1.35	−3.67	−3.39	−2.96	6.43	1.03
SD	1.77	3.38	0.19	0.52	0.44	0.22	0.33	2.08	0.3

Table 2. Estimated parameters, fit errors, and confidence intervals.

15.8 h and 2.7 days, about one order of magnitude lower than those reported by Loomba et al. for HBsAg[59]. The decreased HBeAg life-span predicted by our model may be correlated with the emergence of immune events and/or mutation in the core/precore regions[44] during ARC-520 treatment. Since we have no data on these events, we did not account for them in our model. Production rates of HBsAg and HBeAg are estimated to be $p_S = (1.49 \pm 0.37) \times 10^{-3}$ IU/(cell× day) and $p_E = (1.63 \pm 0.56) \times 10^{-4}$ IU/(cell× day), respectively.

We estimate high efficacy rates, $\epsilon_T > 99.88\%$, for the combined entecavir and ARC-520 effects in blocking HBV DNA synthesis. The additional time-dependent inhibitory effect on intracellular HBV DNA synthesis is on average $g = 0.029 \pm 0.018$ per day.

The estimated $k_{eo} = 0.07 \pm 0.021$ per day, predicts slow transport of ARC-520 from plasma to liver. The half-maximal quantities are small, with average $\log_{10}(EC_2) = -3.38 \pm 0.22$ and $\log_{10}(EC_3) = -2.98 \pm 0.0.33$ for the ARC-520 effects on HBsAg and HBeAg, respectively. This implies that the effects of ARC-520 are long-lived, as suggested by Schluep et al.[56] who found that RNA inhibitors persist and induce antiviral effects for longer than the drug's life-span.

	p	α	p_S	p_E
			$(\times 10^{-3})$	$(\times 10^{-4})$
703	1.99	1206.9	1.54	2.48
704	1.22	861.66	0.85	1.33
708	0.67	613.66	1.65	0.99
710	2.8	1569.85	1.63	1.77
711	9.37	4526.23	1.77	1.58
MEAN	3.21	1755.66	1.49	1.63
MEDIAN	1.99	1206.9	1.63	1.58
SD	3.54	1590.21	0.37	0.56

Table 3. Parameters obtained from fitted parameters in Table 2, under equilibrium conditions defined by Eq. (6).
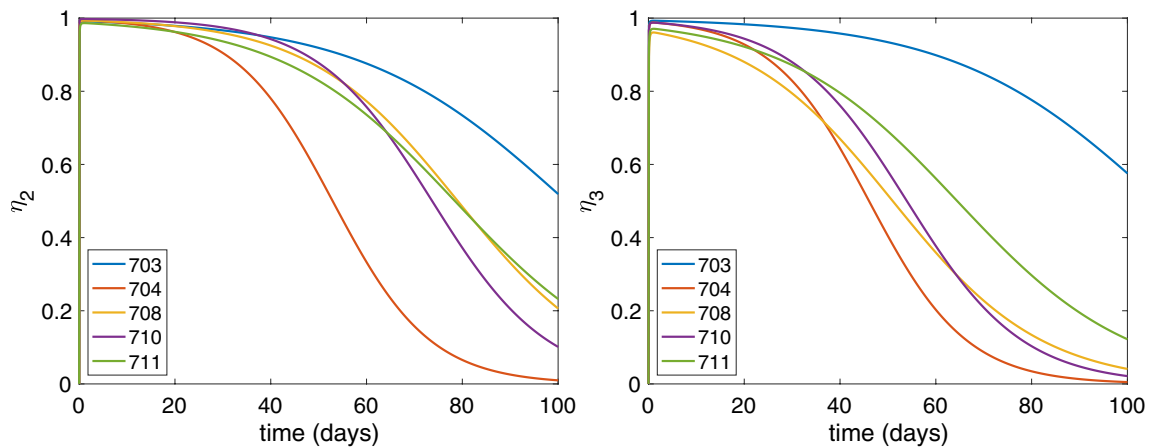
Figure 5. Efficacy of ARC-520 treatment over time as given by model (4) on (**a**) HBsAg production, and (**b**) HBeAg production. The parameters are given in Tables 1 and 2.

Pharmacokinetic–pharmacodynamic model dynamics. The predicted HBV DNA populations as given by model (5) for the estimated parameters follow a biphasic decay with short and sharp first phase corresponding to the removal of HBV DNA followed by long and slow second phase decay due to time dependent treatment induced inhibition of intracellular HBV DNA synthesis and infected cell loss. HBsAg and HBeAg decay at steep rates during the first 24.67 ± 10.2 and 7.64 ± 3.95 days, respectively. After reaching minimum values, on average 1.57 ± 0.19 and 1.6 ± 0.33 orders of magnitude smaller than their initial levels, HBsAg and HBeAg rebound (see Figs. 3 and 4). Once the effects of ARC-520 have completely waned, HBsAg and HBeAg decay at rate δ.

For the estimated parameters, ARC-520 effects η_2 and η_3 given by model (4) increase from 0 to their maximum values during the first $(\ln(k_{eo}) - \ln(d))/(k_{eo} - d) = 1.04 \pm 0.07$ days. The effect of ARC-520 on HBsAg is similar for all patients, with maximal effect at day 1 (ranging between $\eta_2 = 0.986$ and $\eta_2 = 0.998$), which wanes to $\eta_2 = 0.5$ in 1.8 to 3.4 months (see Fig. 5, left panel). The maximal effect of ARC-520 on HBeAg at day 1 ranges between $\eta_3 = 0.96$ (patient 708) and $\eta_3 = 0.993$ (patient 703) and wanes to $\eta_3 = 0.5$ within 1.5 to 3.5 months (see Fig. 5, right panel). For both HBsAg and HBeAg, the effect of ARC-520 lasts longest in patient 703.

In-silico knockout experiments. We are interested in understanding the individual and combined effects of ETV and one-dose of ARC-520 on the dynamics of HBV DNA, HBsAg and HBeAg as given by model (5). We consider the following about the combined ETV and ARC-520 effects on reducing intracellular synthesis, ϵ_T: we either attribute it to ETV alone, $\epsilon_T = \epsilon_T^{ETV}$; or split it between the two effects, $\epsilon_T = \epsilon_T^{both}$. Using the parameters obtained from fitting the combination therapy model (5) to the Heparc-2001 clinical trial data[20], we conduct *in silico* experiments to determine how the dynamics change under: *in silico* monotherapy with entecavir, described by $\eta_i(t) = 0$ for $i = 2, 3$, $g \neq 0$, and $\epsilon_T^{ETV} \neq 0$; and combined entecavir and ARC-520 treatment, described by $\eta_i(t) \neq 0$ for $i = 2, 3$, $g \neq 0$, and $\epsilon_T \neq 0$ ($\epsilon_T^{ETV} \neq 0$, $\epsilon_T^{ARC} \neq 0$, and $\epsilon_T^{both} \neq 0$) obtained through data fitting.

When we investigate *in silico* ETV monotherapy targeting HBV DNA intracellular synthesis, $\epsilon_T = \epsilon_T^{ETV}$, we can analytically derive the solutions of model (5) by considering $\eta_2 = \eta_3 = 0$. $g \neq 0$, and $\epsilon_T = \epsilon_T^{ETV} \neq 0$. The infected cell population becomes $I(t) = I_0 e^{-\delta t}$, the intracellular HBV DNA:
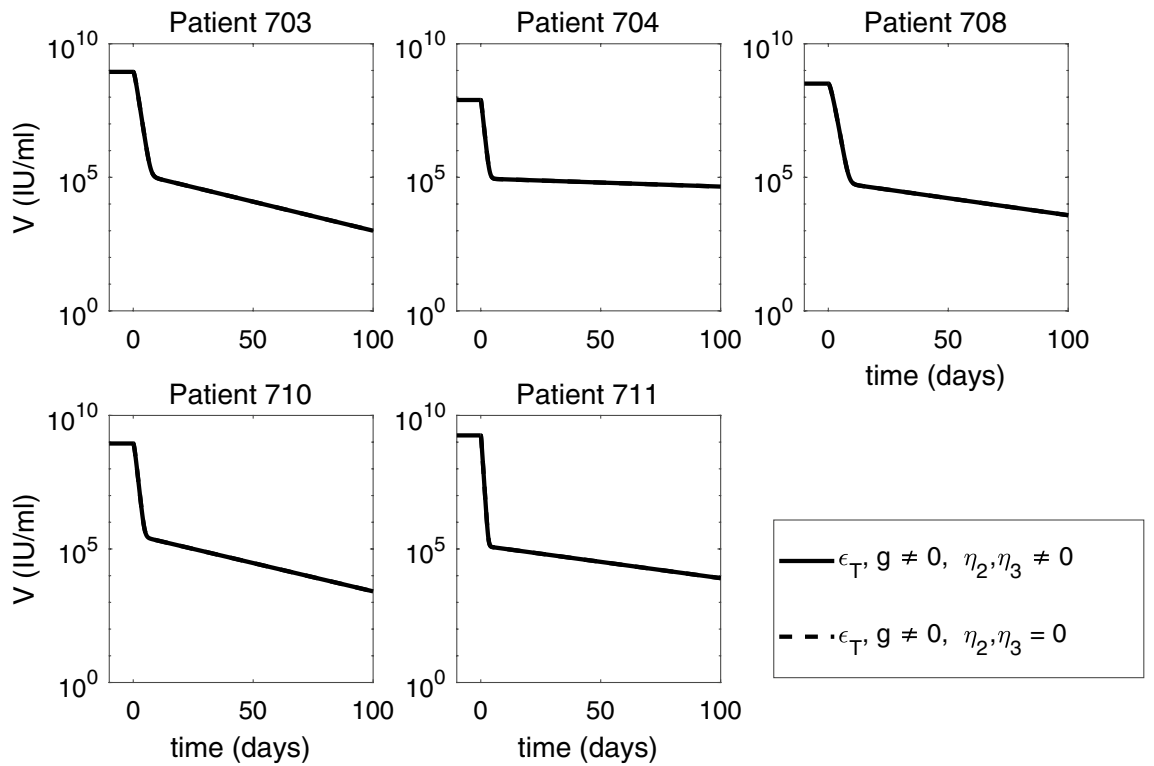
Figure 6. Short-term HBV DNA dynamics under ETV monotherapy (dashed curves), and combined ETV and ARC-520 therapy (solid curves), as given by model (5). Parameters are given in Tables 1 and 2. Additionally, $g \neq 0, \epsilon_T = \epsilon_T^{ETV} \neq 0$ and $\eta_2(t) = \eta_3(t) = 0$ for ETV monotherapy. Note that both axes are plotted on log scale and that the two graphs overlap.

$$D(t) = \frac{(1-\epsilon_T^{ETV})\alpha}{p+c_D-g}e^{-gt} + \left(D_0 - \frac{(1-\epsilon_T^{ETV})\alpha}{p+c_D-g}\right)e^{-(p+c_D)t}, \tag{9}$$

and extracellular HBV DNA:

$$V(t) = \xi p I_0 \left[\frac{(1-\epsilon_T^{ETV})\alpha}{(p+c_D-g)(c-g-\delta)}e^{-(g+\delta)t} + \frac{D_0 - \frac{(1-\epsilon_T^{ETV})\alpha}{p+c_D-g}}{c-p-c_D-\delta}e^{-(p+c_D+\delta)t} \right]$$

$$+ \left(V_0 - \xi p I_0 \left[\frac{(1-\epsilon_T^{ETV})\alpha}{(p+c_D-g)(c-g-\delta)} + \frac{D_0 - \frac{(1-\epsilon_T^{ETV})\alpha}{p+c_D-g}}{c-p-c_D-\delta} \right] \right)e^{-ct}. \tag{10}$$

The equations for HBeAg is given by:

$$S(t) = \frac{p_S I_0}{d_S - \delta}e^{-\delta t} + \left(S_0 - \frac{p_S I_0}{d_S - \delta}\right)e^{-d_S t} = \frac{S_0}{d_S - \delta}\left(d_S e^{-\delta t} - \delta e^{-d_S t}\right), \tag{11}$$

and for HBeAg is given by:

$$E(t) = \frac{p_E I_0}{d_E - \delta}e^{-\delta t} + \left(E_0 - \frac{p_E I_0}{d_E - \delta}\right)e^{-d_E t} = \frac{E_0}{d_E - \delta}\left(d_E e^{-\delta t} - \delta e^{-d_E t}\right). \tag{12}$$

Note that both $S(t)$ and $E(t)$ are independent of ϵ_T. HBV DNA follows a biphasic decay with short and sharp first phase corresponding to the removal of free virus followed by a slow second phase decay due to time dependent treatment induced inhibition of intracellular HBV DNA synthesis and removal of infected cells (see Fig. 6, dashed curves). Serum antigen levels remain elevated for all three populations (see Figs. 7 and 8 , dashed curves).

When we consider that the treatment that blocks intracellular HBV DNA synthesis, ϵ_T, comes from both ETV and ARC-520, we recover the solutions of model (5) for combination therapy given by $\eta_2 = \eta_3 \neq 0, g \neq 0$, and $\epsilon_T = \epsilon_T^{both} \neq 0$. Both HBsAg and HBeAg decay at a steep rate during the first 22.7 ± 8.5 and 7.6 ± 4.1 days, respectively. After reaching minimum values, on average 1.5 ± 0.2 and 1.6 ± 0.4 orders of magnitude smaller than their initial levels, HBsAg and HBeAg rebound to their respective ETV monotherapy levels (see Figs. 7 and 8, solid curves).
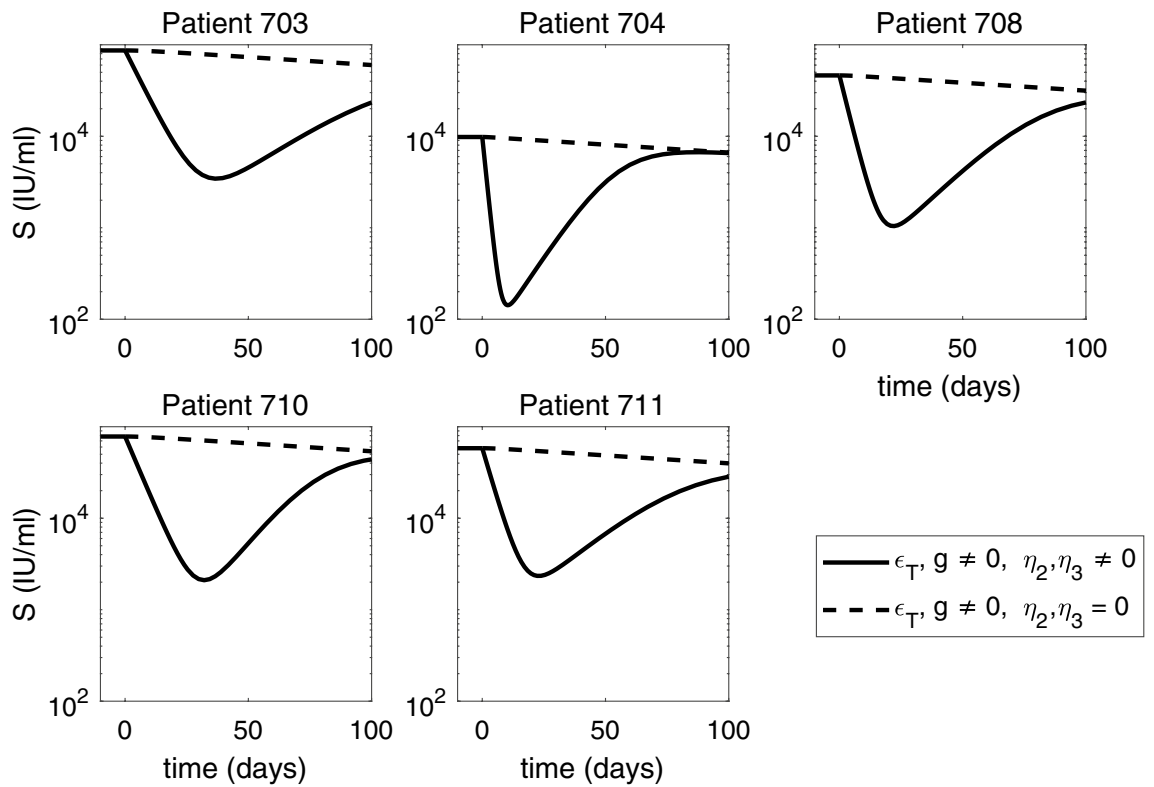
Figure 7. Short-term HBsAg dynamics under ETV monotherapy (dashed curves), and combined ETV and ARC-520 therapy (solid curves), as given by model (5). Parameters are given in Tables 1 and 2. Additionally, $g \neq 0, \epsilon_T = \epsilon_T^{ETV} \neq 0$ and $\eta_2(t) = \eta_3(t) = 0$ for ETV monotherapy. Note that both axes are plotted on log scale.

Sensitivity of model predictions with respect to changes in the infected cell population's initial condition.

Previous estimates for the percentage of HBV-infected hepatocytes vary between $18 \pm 12\%$ in chronic HBsAg carriers[50,51] and 99% in acute infections[26,52]. We have derived our results by assuming that during chronic HBeAg-positive cases half of the liver is infected. Here, we investigate how changes in the size of the initial infected cell population alter our predictions. Analytical investigations show that the dynamics of the viral proteins HBsAg and HBeAg are not influenced by the initial size of the infected cell population, I_0. After treatment initiation $I(t) = I_0 e^{-\delta t}$, and $p_S = d_S S_0/I_0$ and $p_E = d_E E_0/I_0$ (based on the equilibrium assumption (6)). Therefore, the equations for S and E:

$$\frac{dS}{dt} = (1 - \eta_2(t))p_S I - d_S S = (1 - \eta_2(t))d_S S_0 e^{-\delta t} - d_S S_0, \tag{13}$$

and

$$\frac{dE}{dt} = (1 - \eta_3(t))p_E I - d_E E = (1 - \eta_3(t))d_E E_0 e^{-\delta t} - d_E E_0, \tag{14}$$

are independent of I_0. Moreover, for $p = cV_0/(\xi D_0 I_0)$ and $D_0 = 225/(I_0/T_{max})$ we find that intracellular HBV DNA D depends on I_0 (see Fig. 9) but HBV DNA in serum does not.

Long-term predictions and the need for uninfected hepatocyte dynamics

We assumed above that infected hepatocytes have a fixed life-span of 250 days. In this section, we are relaxing this assumption and investigate long-term HBV DNA and HBsAg dynamics when increased hepatocyte loss (due to either drug toxicity, or immune-mediated killing) is being considered. When we model it by increasing the infected cell death rate δ in (5) we obtain the following: long-term dynamics of S and E under ETV monotherapy predict that HBsAg decreases below 1 IU/ml 5.32 ± 0.54 months for $\delta = 7 \times 10^{-2}$ per day, 4.21 ± 0.35 years for $\delta = 7 \times 10^{-3}$ per year, and 7.35 ± 0.61 years for $\delta = 4 \times 10^{-3}$ per day, following the initiation of therapy. Since ETV and other nucleoside analogues do not trigger cccDNA removal (and consequently HBsAg and HBeAg removal), the fast loss of HBsAg predicted by model (5) for higher killing rates δ is not realistic. In this section, we include the dynamics of uninfected and infected cell populations and investigate changes in predictions for increased killing rate δ We incorporate uninfected hepatocytes T which get infected by free virus at rate β, as modeled previously[26,39,63]. Note that we ignore the age of the infection and assume that once a cell becomes infected, it is producing virus (for a PDE model extension in a hepatitis C virus infection, see[64,65]). Both
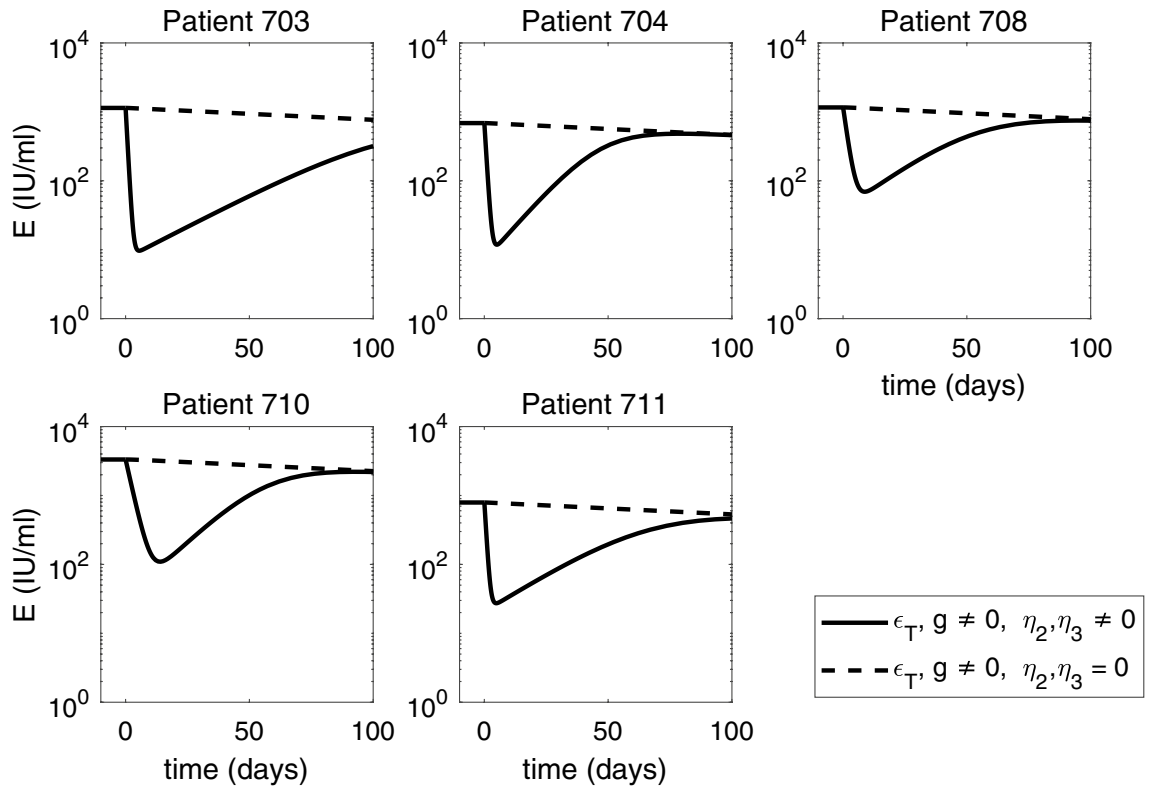
Figure 8. Short-term HBeAg dynamics under ETV monotherapy (dashed curves), and combined ETV and ARC-520 therapy (solid curves), as given by model (5). Parameters are given in Tables 1 and 2. Additionally, $g \neq 0, \epsilon_T = \epsilon_T^{ETV} \neq 0$ and $\eta_2(t) = \eta_3(t) = 0$ for ETV monotherapy. Note that both axes are plotted on log scale.
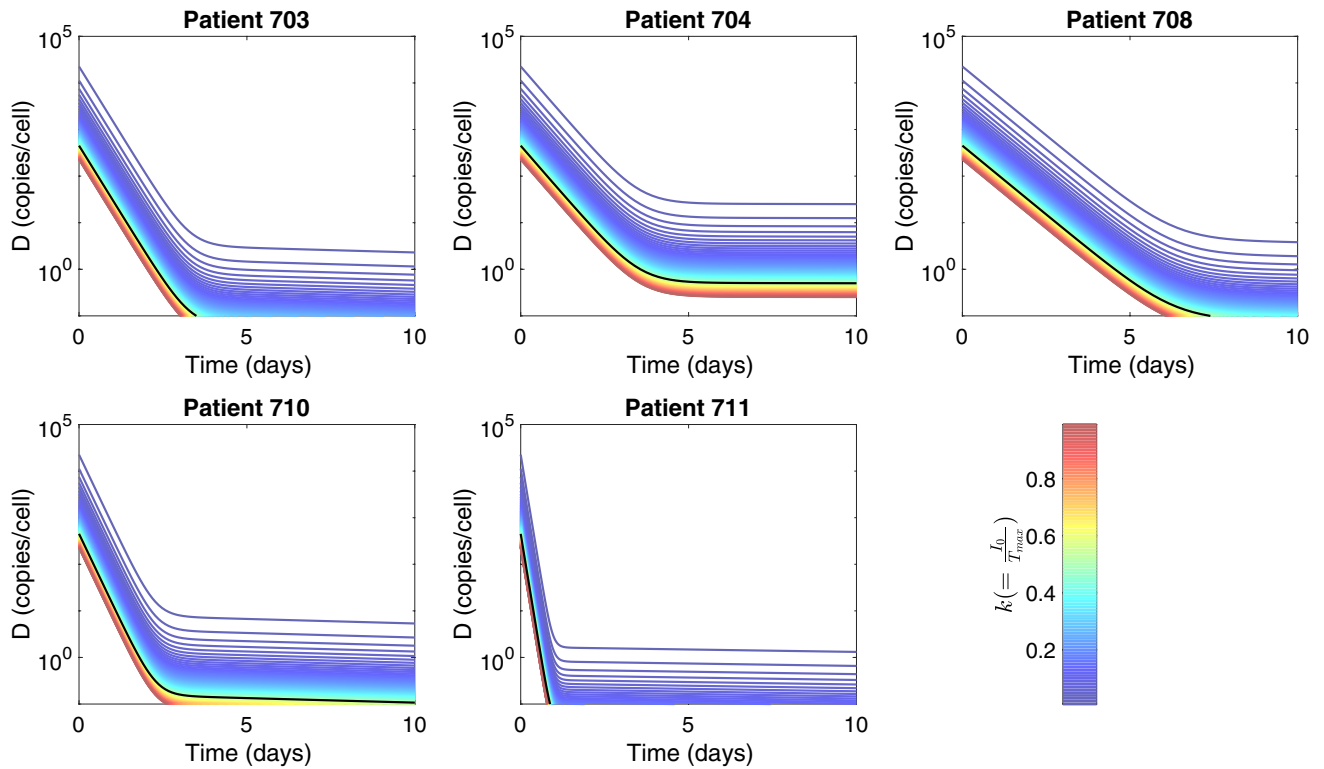

Figure 9. Intracellular HBV DNA dynamics of model (5) for $0.01 < k < 0.99$ and $I_0 = kT_{max}$. Solid black lines show the dynamics for $I_0 = 0.5T_{max}$, which was used in data fitting. Other parameters used are given in Tables 1, 2, and $D_0 = 225/(I_0/T_{max})$.
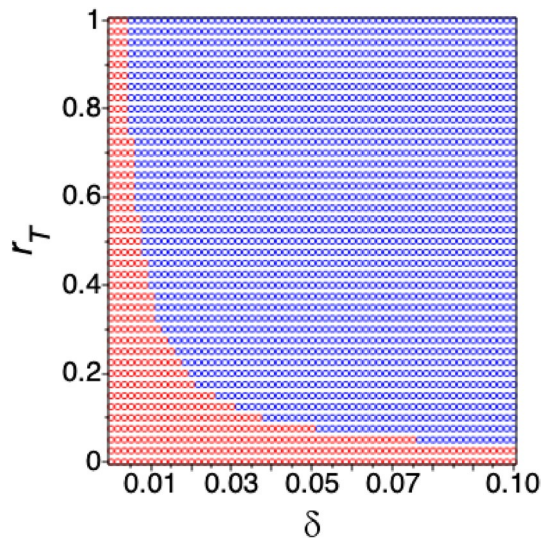
Figure 10. (δ, r_T) ranges where infected cells given by model (15) are cleared (blue dots) or persist (red dots) under ETV monotherapy. Here $r_1 = 1$ per day, $\beta = 10^{-9}$ ml/(IU× day), $d_T = 4 \times 10^{-3}$ per day, initial conditions T_0 and I_0 are set such that the model is in chronic equilibrium in the absence of treatment. The other parameters are given in Tables 1 and 2 for patient 703.

uninfected and infected hepatocytes proliferate according to a logistic term with maximal growth rate r_T and r_I and carrying capacity T_{max}. In chronic HBV infections, cccDNA persist under long-term nucleoside analogues treatment[66]. Since the average cccDNA number of untreated HBeAg positive patients is 2.58 copies per infected cell[54], infected hepatocytes may have two infected off springs. On the other hand, it has been suggested that cccDNA is destabilized by cell division or even lost during mitosis[66]. We account for this by assuming that a fraction Φ of proliferating infected hepatocytes have one infected and one uninfected offspring, and the remaining infected hepatocytes have two infected offsprings. The new model is given by:

$$\frac{dT}{dt} = (r_T T + r_I \Phi I)\left(1 - \frac{T+I}{T_{max}}\right) - \beta TV - d_T T,$$

$$\frac{dI}{dt} = r_I(1-\Phi)I\left(1 - \frac{T+I}{T_{max}}\right) + \beta TV - \delta I,$$

$$\frac{dD}{dt} = (1-\epsilon_T)e^{-gt}\alpha - (p + c_D)D,$$

$$\frac{dV}{dt} = \xi pDI - cV, \qquad\qquad (15)$$

$$\frac{dS}{dt} = (1-\eta_2(t))p_S I - d_S S,$$

$$\frac{dE}{dt} = (1-\eta_3(t))p_E I - d_E E.$$

Liver regenerates rapidly after injury. To account for fast proliferation during chronic disease, we assume that hepatocytes' maximum proliferation rate is $r_T \leq 1$ per day, and $r_I = 1$ per day, corresponding to doubling time of (up to) 16 h[26,67]. The infectivity rate is at the lower end of previously fitted values[11], $\beta = 10^{-9}$ IU/(ml× day); we include a death rate for the uninfected hepatocyte population, $d_T = 4 \times 10^{-3}$ per day[68], identical to that in model (5); and set the fraction of infected hepatocytes that have one uninfected and one infected offspring to $\Phi = 0.05$. Initial conditions of uninfected and infected hepatocytes are set such that the model is in equilibrium prior to treatment with $D_0 = 450$, and V_0, S_0, and E_0 as in Table 1. This leads to almost all hepatocytes being infected.

Without loss of generality, we investigate the dynamics for patient 703 under combination therapy for a continuum of δ values. Our hypothesis is that NA monotherapy cannot lead to HBsAg loss. In order to obtain infected cell persistence (under NA monotherapy), we need to decrease r_T (for a fixed $r_I = 1$) as δ increases (a $r_T - \delta$ threshold required for infected cells persistence is given in Fig. 10). Therefore, HBsAg persistence under increased infected cell killing (as seen in NA treatment) may be explained by high ratio of infected to uninfected cell proliferation. Other events, such as HBV DNA integration, adaptive immune responses, such as cytolytic and non-cytolytic effects, and/or antibody neutralization[11,26] may also explain HBsAg persistence under infected cell (and potentially cccDNA) loss. This is especially true for HBeAg negative patients and NA experienced, HBeAg-positive patients.

Discussion

Reaching functional cure with current anti-HBV therapies in patients with chronic hepatitis B infection is hindered difficult by the lack of approved direct anti-HBsAg treatment and the presence of large numbers of HBsAg in the blood of infected patients[69,70]. Therapies silencing viral translation through RNA interference technology[17,20,21,71], inhibiting HBsAg release via nucleic acid polymers[72–74], and inducing neutralization of HBsAg via specific antibodies[75,76] have shown different levels of success[69,70]. Understanding the relative effects in reducing HBV DNA, HBsAg and HBeAg titers of these new approaches alone, and in combination with traditional nucles(t)ide analogues, is particularly important in informing the development of new generation anti-HBsAg therapies.

To help in this endeavor, we developed mathematical models describing the HBV DNA, HBsAg and HBeAg in the presence of a silencing RNAi drug called ARC-520. We used the models and clinical trial data from treatment naive, HBeAg-positive patients that receive a one time ARC-520 injection and daily nucleoside analogue treatment with entecavir[20], to determine the efficacy of ARC-520 and nucleoside therapies on the short and long-term dynamics of HBV DNA, HBsAg, and HBeAg. To the best of our knowledge, we report for the first time that the time-dependent ARC-520 effects on HBsAg and HBeAg are more than 96% effective around day 1, and slowly wane to 50% in 1.8-3.4 months and 1.5-3.5 months, respectively. The combined ARC-520 and entecavir effect on HBV DNA is constant over time, with efficacy of more than 99.8%, which is similar to other nucleoside analogues trials.

A simplified version of the model, which ignored the dynamics of hepatocyte proliferation and infection, was sufficient to explain the short-term (about 100 days) dynamics observed in five patients in the current study. In the long-term, however, infected cells may die at faster rates, due to either drug toxic effects or increased immune killing. Lowering infected hepatocyte's life-span to 100 (10) days, however, resulted in fast HBsAg removal, with decay below 1 IU/ml in 4.2 years (5.3 months). This loss, however, was in contradiction with clinical reports of low percentages of patients clearing HBsAg during long-term nucleoside analogues treatment[6], suggesting that more complex models are needed for long-term (several years) predictions. To determine under what conditions increased infected cells death does not spill over into unrealistic HBsAg and HBeAg loss under long-term nucleoside analogue therapy, we extended model (5) to include infected and uninfected cell dynamics. We assumed lower infected cells life-span (100 and 10 days), included division of both infected and uninfected populations, and determined that long-term HBsAg and HBeAg persistence under long-term HBV DNA clearance can be explained by high ratios of infected to uninfected division rates. Therefore, high ratio of infected to uninfected division rates, which correspond to the infection of the entire liver and may be indicative of scenarios where HBsAg seroclearance will not happen. Interestingly, we and others have associated high ratios of infected to uninfected division rates to triphasic HBV DNA decay under treatments with nucleoside analogues, a sign of suboptimal drug response[33,35]. Whether infected hepatocytes indeed proliferate faster than uninfected hepatocytes remains under investigation.

While modeling results suggest that one-dose of ARC-520, in combination of daily entecavir, has limited long-term effects, we did not consider whether a transient reduction of HBsAg and HBeAg leads to the appearance of anti-HBs or anti-HBe antibodies, removal of immune-exhaustion, and eventual functional cure. Recent studies found that large levels of HBsAg might cause dysfunctional programming of HBsAg-specific B cells through persistent stimulation[77]. It has been suggested that therapeutic vaccines containing one (PreS2) or two (PreS1 or PreS2) envelope proteins together with serum HBsAg reducing drug therapies are needed in order to induce high levels of anti-HB antibodies, which may correlate with functional cure[78–80]. We ignored the level of immune modulation following RNAi based therapy, such as cytolytic and non-cytolytic T cell functions and antibody responses, which is a model limitation, and therefore, we cannot say whether such effects were induced at higher rates during the transient HBsAg loss.

Our study has limitations. We only used the data on HBeAg-positive patients (cohort 7 in[20]) since they best responded to ARC-520 therapy. Moreover, we did not model HBV DNA integration, which has been reported as a source of HBsAg production, especially in HBeAg-negative and NA-experienced HBeAg-positive patients with low cccDNA[20]. As kinetic HBV data from next generation RNAi therapy capable of inducing stronger HBsAg reduction in both HBeAg-negative and HBeAg-positive patients becomes available[21,81,82], we aim to adapt our modeling framework to include HBV DNA integration.

In conclusion, we developed a mathematical model and used it together with patient data, to estimate the time-dependent ARC-520 efficacies in blocking HBsAg and HBeAg productions. Additional data and theoretical efforts are needed to determine whether RNAi therapies have a feedback effect on the reversal of immune exhaustion, immunomodulatory immune responses, and potential functional cure.

References

1. Rijckborst, V. & Janssen, H. L. The role of interferon in hepatitis B therapy. *Curr. Hepat. Rep.* **9**, 231–238 (2010).
2. Zhang, Y. *et al.* Combination therapy based on pegylated interferon alfa improves the therapeutic response of patients with chronic hepatitis B who exhibit high levels of hepatitis B e-antigen at 24 weeks: a retrospective observational study. *Medicine* **98**, e17022 (2019).
3. Razavi-Shearer, D. *et al.* Global prevalence, treatment, and prevention of hepatitis B virus infection in 2016: a modelling study. *Lancet Gastroenterol. Hepatol.* **3**, 383–403 (2018).
4. Chu, C.-M. & Liaw, Y.-F. Hepatitis B surface antigen seroclearance during chronic HBV infection. *Antivir. Ther.* **15**, 133–143 (2010).
5. Zhang, W. *et al.* Consensus on pegylated interferon alpha in treatment of chronic hepatitis B. *J. Clin. Transl. Hepatol.* **6**, 1 (2018).
6. Agarwal, K. *et al.* EASL 2017: clinical practice guidelines on the management of hepatitis B virus infection. *J. Hepatol.* **67**, 370–398 (2017).

7. Fung, J. *et al.* Nucleoside/nucleotide analogues in the treatment of chronic hepatitis B. *J. Antimicrob. Chemother.* **66**, 2715–2725 (2011).

8. Papatheodoridis, G. *et al.* Discontinuation of oral antivirals in chronic hepatitis B: a systematic review. *Hepatology* **63**, 1481–1492 (2016).

9. Chen, M. T. *et al.* A function of the hepatitis B virus precore protein is to regulate the immune response to the core antigen. *Proc. Natl. Acad. Sci. USA* **101**, 14913–14918 (2004).

10. Prange, R. Host factors involved in hepatitis B virus maturation, assembly, and egress. *Med. Microbiol. Immunol.* **201**, 449–461 (2012).

11. Ciupe, S. M., Ribeiro, R. M. & Perelson, A. S. Antibody responses during hepatitis B viral infection. *PLoS Comput. Biol.* **10**, e1003730 (2014).

12. Wieland, S. F. & Chisari, F. V. Stealth and cunning: hepatitis B and hepatitis C viruses. *J. Virol.* **79**, 9369–9380 (2005).

13. Bertoletti, A. & Ferrari, C. Innate and adaptive immune responses in chronic hepatitis B virus infections: towards restoration of immune control of viral infection. *Gut* **61**, 1754–1764 (2012).

14. Neumann, A. U. *et al.* Novel mechanism of antibodies to hepatitis B virus in blocking viral particle release from cells. *Hepatology* **52**, 875–885 (2010).

15. Vaillant, A. Rep 2139: antiviral mechanisms and applications in achieving functional control of HBV and HDV infection. *ACS Infect. Dis.* **5**, 675–687 (2018).

16. Setten, R. L., Rossi, J. J. & Han, S.-P. The current state and future directions of RNAi-based therapeutics. *Nat. Rev. Drug Discov.* **18**, 421–446 (2019).

17. Wooddell, C. I. *et al.* Hepatocyte-targeted RNAi therapeutics for the treatment of chronic hepatitis B virus infection. *Mol. Ther.* **21**, 973–985 (2013).

18. Xia, Y. & Liang, T. J. Development of direct-acting antiviral and host-targeting agents for treatment of hepatitis B virus infection. *Gastroenterology* **156**, 311–324 (2019).

19. Trubetskoy, V. S. *et al.* Phosphorylation-specific status of RNAi triggers in pharmacokinetic and biodistribution analyses. *Nucleic Acids Res.* **45**, 1469–1478 (2017).

20. Wooddell, C. I. *et al.* RNAi-based treatment of chronically infected patients and chimpanzees reveals that integrated hepatitis B virus DNA is a source of HBsAg. *Sci. Transl. Med.* **9**, eaan0241 (2017).

21. Yuen, M.-F. *et al.* RNA interference therapy with ARC-520 results in prolonged hepatitis B surface antigen response in patients with chronic hepatitis B infection. *Hepatology* **72**, 19–31 (2020).

22. Van den Berg, F. *et al.* Advances with RNAi-based therapy for hepatitis B virus infection. *Viruses* **12**, 851 (2020).

23. Tang, L., Kottilil, S. & Wilson, E. Strategies to eliminate HBV infection: an update. *Future Virol.* **15**, 35–51 (2020).

24. French, J., Locarnini, S. & Zoulim, F. Direct-acting antivirals and viral rna targeting for hepatitis B cure. *Curr. Opin. HIV AIDS* **15**, 165–172 (2020).

25. Nowak, M. *et al.* Viral dynamics in hepatitis B virus infection. *Proc. Natl. Acad. Sci. USA* **93**, 4398–4402 (1996).

26. Ciupe, S. *et al.* The role of cells refractory to productive infection in acute hepatitis B viral dynamics. *Proc. Natl. Acad. Sci. USA* **104**, 5050–5055 (2007).

27. Goyal, A., Ribeiro, R. M. & Perelson, A. S. The role of infected cell proliferation in the clearance of acute HBV infection in humans. *Viruses* **9**, 350 (2017).

28. Ciupe, S. M. Modeling the dynamics of hepatitis B infection, immunity, and drug therapy. *Immunol. Rev.* **285**, 38–54 (2018).

29. Ciupe, S. M., Catllá, A. J., Forde, J. & Schaeffer, D. G. Dynamics of hepatitis B virus infection: what causes viral clearance?. *Math. Popul. Stud.* **18**, 87–105 (2011).

30. Ji, Y. *et al.* A mathematical model for anti-HBV infection treatment with lamivudine and curative effect prediction. In *Control and Automation, 2007. ICCA 2007. IEEE International Conference on*, 2485–2488 (IEEE, 2007).

31. Gourley, S., Kuang, Y. & Nagy, J. Dynamics of a delay differential model of hepatitis B virus. *J. Biol. Dyn.* **2**, 140–53 (2008).

32. Eikenberry, S. *et al.* The dynamics of a delay model of HBV infection with logistic hepatocyte growth. *Math. Biosci. Eng.* **6**, 283–99 (2009).

33. Dahari, H. *et al.* Modeling complex decay profiles of hepatitis B virus during antiviral therapy. *Hepatology* **49**, 32–38 (2009).

34. Lewin, S. R. *et al.* Analysis of hepatitis B viral load decline under potent therapy: complex decay profiles observed. *Hepatology* **34**, 1012–1020 (2001).

35. Carracedo Rodriguez, A., Chung, M. & Ciupe, S. M. Understanding the complex patterns observed during hepatitis B virus therapy. *Viruses* **9**, 117 (2017).

36. Goyal, A. & Murray, J. M. Modelling the impact of cell-to-cell transmission in hepatitis B virus. *PLoS ONE* **11**, e0161978 (2016).

37. Murray, J. M. & Goyal, A. In silico single cell dynamics of hepatitis B virus infection and clearance. *J. Theor. Biol.* **366**, 91–102 (2015).

38. Goyal, A. & Chauhan, R. The dynamics of integration, viral suppression and cell-cell transmission in the development of occult hepatitis B virus infection. *J. Theor. Biol.* **455**, 269–280 (2018).

39. Ciupe, S. *et al.* Modeling the mechanisms of acute hepatitis B virus infection. *J. Theor. Biol.* **247**, 23–35 (2007).

40. Long, C., Qi, H. & Huang, S.-H. Mathematical modeling of cytotoxic lymphocyte-mediated immune response to hepatitis B virus infection. *J. Biomed. Biotechnol.* **2008**, 1–9 (2008).

41. Kim, H. *et al.* Mathematical modeling of triphasic viral dynamics in patients with HBeAg-positive chronic hepatitis B showing response to 24-week clevudine therapy. *PLoS ONE* **7**, e50377 (2012).

42. Yousfi, N., Hattaf, K. & Tridane, A. Modeling the adaptive immune response in HBV infection. *J. Math. Biol.* **63**, 933–957 (2011).

43. Hews, S. *et al.* Rich dynamics of a hepatitis B viral infection model with logistic hepatocyte growth. *J. Math. Biol.* **60**, 573–590 (2010).

44. Kadelka, S. & Ciupe, S. M. Mathematical investigation of HBeAg seroclearance. *Math. Biosci. Eng.* **16**, 7616–7658 (2019).

45. National Clinical Guideline Centre, UK. Hepatitis B (chronic): diagnosis and management of chronic hepatitis B in children, young people and adults (2013).

46. Uchida, T. *et al.* Persistent loss of hepatitis B virus markers in serum without cellular immunity by combination of peginterferon and entecavir therapy in humanized mice. *Antimicrob. Agents Chemother.* **61**, e00725-17 (2017).

47. Canini, L. *et al.* Understanding hepatitis B virus dynamics and the antiviral effect of interferon-alpha treatment in humanized chimeric mice. *bioRxiv* (2020).

48. Gabrielsson, J. & Weiner, D. *Pharmacokinetic and Pharmacodynamic Data Analysis: Concepts and Applications* (CRC Press, Boca Raton, 2001).

49. Felmlee, M. A., Morris, M. E. & Mager, D. E. Mechanism-based pharmacodynamic modeling. In *Computational Toxicology*, 583–600 (Springer, 2012).

50. Volz, T. *et al.* Impaired intrahepatic hepatitis B virus productivity contributes to low viremia in most HBeAg-negative patients. *Gastroenterology* **133**, 843–852 (2007).

51. Rodríguez-Iñigo, E. *et al.* Distribution of hepatitis B virus in the liver of chronic hepatitis C patients with occult hepatitis B virus infection. *J. Med. Virol.* **70**, 571–580 (2003).

52. Guidotti, L. G. *et al.* Viral clearance without destruction of infected cells during acute HBV infection. *Science* **284**, 825–829 (1999).

53. Sherlock, S. *et al.* *Diseases of the Liver and Biliary System* (Wiley, Hoboken, 2002).

54. Wursthorn, K. *et al.* Peginterferon alpha-2b plus adefovir induce strong cccDNA decline and hbsag reduction in patients with chronic hepatitis B. *Hepatology* **44**, 675–684 (2006).

55. Xu, C. *et al.* Interferons accelerate decay of replication-competent nucleocapsids of hepatitis B virus. *J. Virol.* **84**, 9332–9340 (2010).

56. Schluep, T. *et al.* Safety, tolerability, and pharmacokinetics of ARC-520 injection, an rna interference-based therapeutic for the treatment of chronic hepatitis B virus infection, in healthy volunteers. *Clin. Pharmacol. Drug Dev.* **6**, 350–362 (2017).

57. Ishida, Y. *et al.* Acute hepatitis B virus infection in humanized chimeric mice has multiphasic viral kinetics. *Hepatology* **68**, 473–484 (2018).

58. Dandri, M. *et al.* Virion half-life in chronic hepatitis B infection is strongly correlated with levels of viremia. *Hepatology* **48**, 1079–1086 (2008).

59. Loomba, R. *et al.* Discovery of half-life of circulating hepatitis B surface antigen in patients with chronic hepatitis B infection using heavy water labeling. *Clin. Infect. Dis.* **69**(3), 542–545 (2019).

60. Shekhtman, L. *et al.* Modelling hepatitis D virus RNA and HBsAg dynamics during nucleic acid polymer monotherapy suggest rapid turnover of HBsAg. *Sci. Rep.* **10**, 1–7 (2020).

61. Ciupe, S. M. & Hews, S. Mathematical models of e-antigen mediated immune tolerance and activation following prenatal HBV infection. *PLoS ONE* **7**, e39591 (2012).

62. Whalley, S. A. *et al.* Kinetics of acute hepatitis B virus infection in humans. *J. Exp. Med.* **193**, 847–854 (2001).

63. Nowak, M. A. *et al.* Viral dynamics in hepatitis B virus infection. *Proc. Natl. Acad. Sci. USA* **93**, 4398–4402 (1996).

64. Rong, L. *et al.* Analysis of hepatitis C virus decline during treatment with the protease inhibitor danoprevir using a multiscale model. *PLoS Comput. Biol.* **9**, e1002959 (2013).

65. Churkin, A., Lewkiewicz, S., Reinharz, V., Dahari, H. & Barash, D. Efficient methods for parameter estimation of ordinary and partial differential equation models of viral hepatitis kinetics. *Mathematics* **8**, 1483 (2020).

66. Allweiss, L. & Dandri, M. The role of cccDNA in HBV maintenance. *Viruses* **9**, 156 (2017).

67. Lodish, H. *et al. Molecular Cell Biology* (Macmillan, New York, 2008).

68. Duncan, A. W., Dorrell, C. & Grompe, M. Stem cells and liver regeneration. *Gastroenterology* **137**, 466–481 (2009).

69. Dusheiko, G. & Wang, B. Hepatitis B surface antigen loss: too little, too late and the challenge for the future. *Gastroenterology* **156**, 548–551 (2019).

70. Lu, M., Ma, Z., Zhang, E., Gao, S. & Xiong, Y. Toward a functional cure for hepatitis B: the rationale and challenges for therapeutic targeting of the B cell immune response. *Front. Immunol.* **10**, 2308 (2019).

71. Gish, R. G. *et al.* Synthetic RNAi triggers and their use in chronic hepatitis B therapies with curative intent. *Antivir. Res.* **121**, 97–108 (2015).

72. Vaillant, A. Nucleic acid polymers: broad spectrum antiviral activity, antiviral mechanisms and optimization for the treatment of hepatitis B and hepatitis D infection. *Antivir. Res.* **133**, 32–40 (2016).

73. Al-Mahtab, M., Bazinet, M. & Vaillant, A. Safety and efficacy of nucleic acid polymers in monotherapy and combined with immunotherapy in treatment-naive Bangladeshi patients with HBeAg+ chronic hepatitis B infection. *PLoS ONE* **11**, e0156667 (2016).

74. Bazinet, M. *et al.* Safety and efficacy of 48 weeks REP 2139 or REP 2165, tenofovir disoproxil, and pegylated interferon alfa-2a in patients with chronic HBV infection naïve to nucleos (t) ide therapy. *Gastroenterology* **158**, 2180–2194 (2020).

75. Dembek, C., Protzer, U. & Roggendorf, M. Overcoming immune tolerance in chronic hepatitis B by therapeutic vaccination. *Curr. Opin. Virol.* **30**, 58–67 (2018).

76. Zhang, T.-Y. *et al.* A unique B cell epitope-based particulate vaccine shows effective suppression of hepatitis B surface antigen in mice. *Gut* **69**, 343–354 (2020).

77. Le Bert, N. *et al.* Comparative characterization of B cells specific for HBV nucleocapsid and envelope proteins in patients with chronic hepatitis B. *J. Hepatol.* **72**(1), 34–44 (2020).

78. Lada, O., Benhamou, Y., Poynard, T. & Thibault, V. Coexistence of hepatitis B surface antigen (HBsAg) and anti-HBs antibodies in chronic hepatitis B virus carriers: influence of "a" determinant variants. *J. Virol.* **80**, 2968–2975 (2006).

79. Shapira, M. Y., Zeira, E., Adler, R. & Shouval, D. Rapid seroprotection against hepatitis B following the first dose of a pre-S1/pre-S2/S vaccine. *J. Hepatol.* **34**, 123–127 (2001).

80. Le Hoa, P. T. *et al.* Randomized controlled study investigating viral suppression and serological response following pre-S1/pre-S2/S vaccine therapy combined with lamivudine treatment in HBeAg-positive patients with chronic hepatitis B. *Antimicrob. Agents Chemother.* **53**, 5134–5140 (2009).

81. Yuen, R. *et al.* Short term rna interference therapy in chronic hepatitis B using JNJ-3989 brings majority of patients to HBsAg< 100 IU/ml threshold. *J. Hepatol.* **70**, e51–e52 (2019).

82. Gane, E. J. *et al.* Dose response with the RNA interference (RNAi) therapy JNJ-3989 combined with nucleos (t) ide analogue (NA) treatment in expanded cohorts of patients (PTS) with chronic hepatitis B (CHB). In *Poster Abstract, AASLD The Liver Meeting, Boston, USA, November 9–13 2019. Hepatoogy* (2019).

Acknowledgements

Author contributions

All authors conceived the study and performed the analyses. S.K. wrote the code. S.K. and S.M.C. wrote the manuscript. All authors reviewed and revised the manuscript.

Competing interests

The authors declare no competing interests.

Additional information

Correspondence and requests for materials should be addressed to S.M.C.

Reprints and permissions information is available at www.nature.com/reprints.

Publisher's note Springer Nature remains neutral with regard to jurisdictional claims in published maps and institutional affiliations.